Curvature Entropy Enhanced Principal Component Analysis for 3D LiDAR Human Head Segmentation

Muhtadin
Department of Electrical Engineering, Institut Teknologi Sepuluh Nopember, Surabaya, Indonesia
muhtadin@its.ac.id

I Ketut Eddy Purnama
Department of Electrical Engineering, Institut Teknologi Sepuluh Nopember, Surabaya, Indonesia
ketut@its.ac.id

Nova Eka Budiyanta
Department of Electrical Engineering, School of Bioscience, Technology, and Innovation, Universitas Katolik Indonesia Atma Jaya, BSD City, Indonesia | Atma Jaya AI Research Center, Universitas Katolik Indonesia Atma Jaya, Jakarta, Indonesia
nova.eka@atmajaya.ac.id

Hanugra Aulia Sidharta
Computer Science Department, School of Computer Science, Bina Nusantara University, Jakarta, Indonesia
hanugra.sidharta@binus.ac.id

Mauridhi Hery Purnomo
Department of Electrical Engineering, Institut Teknologi Sepuluh Nopember, Surabaya, Indonesia
hery@ee.its.ac.id (corresponding author)

Received: 14 January 2026 | Revised: 8 February 2026 and 21 February 2026 | Accepted: 22 February 2026

 DOI: https://doi.org/10.48084/etasr.17551

ABSTRACT

Accurate segmentation of the human head and torso from Three-Dimensional (3D) LiDAR point clouds is essential for applications in human–robot interaction, autonomous navigation, and contactless rehabilitation monitoring. Traditional unsupervised approaches based solely on Principal Component Analysis (PCA) often suffer from instability under pose variation and sensor noise, as the geometric width of the head and shoulders can overlap. This study proposes a novel Curvature Entropy-Enhanced Principal Component Analysis (PCA+CE) framework that combines global geometric width descriptors with local surface CE to achieve robust, unsupervised head–body segmentation. Specifically, a CE term was computed from surface-normal directional randomness and fused adaptively with PCA width through a lightweight weighting-and-thresholding scheme to estimate the head–torso boundary Z_{cut} automatically, without labeled data or learning. Experiments using human subsets of the KITTI Raw 3D LiDAR dataset demonstrate that PCA+CE consistently improves segmentation accuracy over the pure PCA baseline, achieving higher precision, recall, and F1-score. The method yields a 0.36 % increase in overall F1-score from 84.1% to 84.4% while maintaining computational efficiency and full interpretability. These results highlight CE as an effective local stabilizer for lightweight geometric segmentation in sparse LiDAR environments.

Keywords-3D LiDAR segmentation; curvature entropy; geometric modeling; cloud processing; Principal Component Analysis (PCA)

I. INTRODUCTION

3D LiDAR sensing has become a key modality in modern intelligent systems, supporting robust 3D perception for autonomous navigation and localization [1] as well as human detection and tracking in human-centered robotic scenarios [2]. In autonomous driving research, LiDAR-based 3D object detection has been extensively studied, highlighting the value of geometric point-cloud representations for reliable perception [3]. In this context, efficient person-level segmentation and tracking are crucial preprocessing steps for downstream understanding of human presence and motion [2].

While deep-learning-based point-cloud segmentation methods have achieved impressive accuracy [4, 5], lightweight and real-time applications often still favor unsupervised geometric approaches due to their simplicity, interpretability, and reduced data requirements. Among these, PCA is popular for describing spatial variance and cross-sectional shape. By computing the lateral spread (PCA width) along vertical slices, PCA-based models can approximate the geometric transition between the head and torso [6]. However, PCA is sensitive to noise and incomplete shapes [7], and in practice, it can degrade under pose variation, rotation, and LiDAR noise where shoulder and head widths overlap, producing unstable segmentation boundaries across frames and viewing angles [6, 8]. This instability motivates integrating a local geometric descriptor that adapts to micro-level curvature variation while preserving the interpretability of PCA.

Existing solutions attempt to mitigate this issue using either global geometric optimization, for example, point-cloud registration or shape alignment [9], or supervised deep networks for point-cloud feature learning and segmentation [4]. Global optimization models can be sensitive to initialization and variations in acquisition conditions such as viewpoint and sampling irregularities, while supervised deep models typically require annotated training data and incur significant training/inference costs for deployment in real-time pipelines [4, 9]. Meanwhile, robustness-oriented geometric refinements, including neighborhood-reconstruction-based normal estimation, can improve local surface stability, but they do not fully resolve the trade-off between interpretability and robustness to micro-level geometric variation across poses [10]. Therefore, there is a practical gap between model interpretability and robustness to local geometric variation.

To address these challenges, this study proposes a PCA+CE segmentation framework that fuses global and local shape descriptors in an unsupervised formulation. The key idea is that the local curvature distribution of the head differs significantly from that of the torso: head regions exhibit a higher CE score due to their roundness and normal direction variance, whereas torso surfaces are relatively planar. By combining CE with PCA width, the proposed method captures both macro-geometry and micro-curvature, yielding stable vertical boundaries even under pose variation.

A static LiDAR frame is represented as a set of n points using:

$$P = \{p_i = [x_i, y_i, z_i]^T | i = 1, \dots, n\} \quad (1)$$

The segmentation aims to estimate a cut plane $z = z_{cut}$ that separates the head from $z \geq z_{cut}$ from the body. Each frame is processed independently to ensure that the method remains applicable to a single scan or sparse frame system.

A. Main Contribution

The main contributions of the study are:

- Local CE is formulated from the variance of surface normal transitions, representing the directional randomness among neighboring points.
- Feature fusion of normalized PCA width and CE through adaptive weighting to detect stable head–torso transitions under pose variations.
- Adaptive thresholding to maintain robustness against local geometric fluctuations while preserving computational efficiency.

II. GEOMETRIC–CURVATURE SEGMENTATION APPROACHES

Human head–body segmentation from 3D LiDAR point clouds is a central problem in geometric perception and shape understanding. Existing approaches can be grouped into three categories: (1) geometric models based on global descriptors such as PCA, (2) curvature-based surface analysis capturing local shape transitions, and (3) hybrid schemes that integrate global and local cues to balance interpretability and robustness.

A. PCA-Based Geometric Segmentation

PCA has long served as an efficient tool for analyzing spatial variance in 3D point clouds through covariance-based descriptors, underpinning classic operations such as local normal estimation and surface reconstruction from unorganized points [11, 12]. In human body segmentation, PCA is commonly applied in a slice-wise manner along the vertical axis to estimate lateral width, producing a profile that reflects the cross-sectional body structure. Authors in [6, 8] showed that PCA/SVD-based covariance descriptors can be used to identify human head slices in LiDAR data, highlighting the usefulness of simple geometric cues for head–torso separation in practice. However, PCA and eigen descriptors are sensitive to noise and incomplete shapes [7], and PCA-based segmentation often relies on a global variance assumption that the head is narrower than the torso. This assumption can break under rotations or non-frontal poses, where shoulder and head widths overlap, leading to misalignment and unstable cut positions across frames [6, 8].

B. Curvature-Based Surface Analysis

Curvature descriptors capture fine-scale variations of 3D surfaces and are widely used for feature characterization in point-cloud and mesh analysis [13]. In point clouds, curvature-related cues are derived from local covariance eigen-analysis and from estimated surface normals, where the stability of both normals and curvature strongly depends on neighborhood size, sampling density, and noise level [12, 13]. This is particularly problematic for LiDAR point clouds, which are often sparse and non-uniformly sampled. Naïve curvature estimation can either amplify noise or wash out salient boundaries [12]. To

improve robustness, entropy-based formulations, which measure the dispersion or randomness of local surface orientations rather than relying solely on absolute curvature magnitude, have been proposed [14]. Related ideas have also been explored under adaptive CE features to emphasize locally informative regions while reducing sensitivity to sampling artifacts [15]. In this context, such orientation and CE cues are attractive because they can act as stable indicators of local shape irregularity. These cues tend to be higher in rounded, rapidly varying regions and lower in near-planar areas, thereby complementing PCA's global width profile without sacrificing interpretability.

C. Hybrid Fusion Approaches

Hybrid schemes that combine global and local geometric cues have been explored to improve segmentation performance without supervised training. The core idea is to retain the global stability of PCA-derived width profiles while injecting local adaptivity via curvature-related descriptors. In parallel, many pipelines pursue feature fusion through deep learning or graph-based optimization, such as CRF or min-cut formulations, to integrate heterogeneous cues [16–18]. However, these approaches are more computationally demanding and often less interpretable than purely geometric models. In contrast, lightweight, geometry-driven fusion is comparatively underexplored for human LiDAR data in practical settings. To address this gap, the proposed PCA+CE method introduces CE as a local weighting term on the PCA width profile, leveraging entropy-based surface-orientation cues to stabilize slice-wise decisions while preserving interpretability [14, 15].

The literature indicates a practical gap in lightweight LiDAR human segmentation. PCA-based slice-width cues are efficient and interpretable but can drift under pose variation when head and shoulder widths overlap, whereas curvature-based cues capture local shape changes but can be unstable in sparse and non-uniform LiDAR sampling. Hybrid fusion is, therefore, a natural direction; however, many existing fusion pipelines rely on learning or computationally heavier optimization. To address this limitation, the proposed study introduces a fully unsupervised and interpretable PCA+CE fusion framework that injects a local surface irregularity stabilizer into the PCA width profile to improve boundary robustness without training data.

III. METHODOLOGY

The objective of the study is to automatically identify the transition boundary between the human head and torso from 3D LiDAR point cloud data without relying on explicit 3D models or manual annotations. The proposed method leverages both geometric and statistical properties of LiDAR point distributions. Unlike previous studies that relied primarily on geometric width variation along the vertical axis [6], this work introduces a curvature-based descriptor with CE to enhance segmentation robustness. The head–body boundary is detected by analyzing vertical variations of geometric features along the z-axis. The 3D geometric complexity within each vertical slice is quantified through the directional variance of surface normal vectors among neighboring points. The mean directional change Δn represents CE, describing the degree of local surface irregularity. An adaptive thresholding mechanism is then used to automatically estimate the cut height z_{cut}, which separates the head and torso regions. This curvature-entropy-based approach improves robustness against pose variation, uneven sampling density, and sensor orientation noise compared with a pure PCA-based method. The framework consists of six sequential stages, as illustrated in Figure 1.

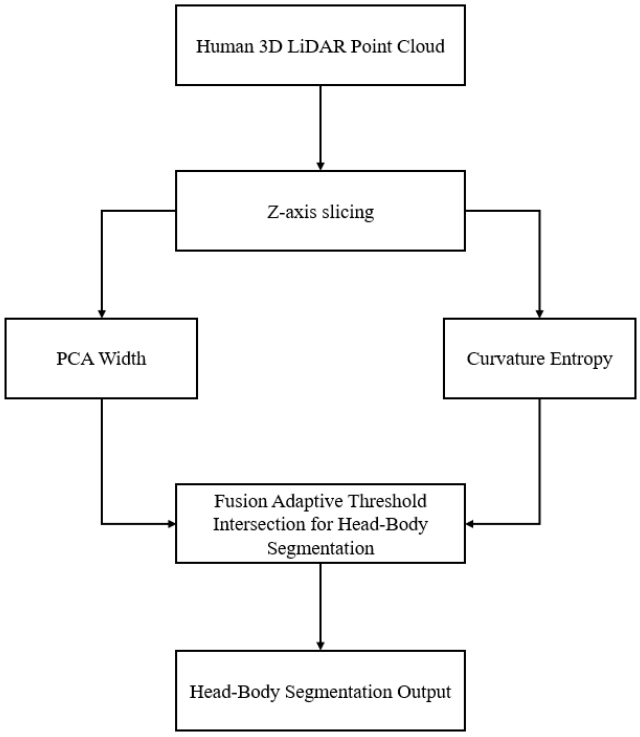

Fig. 1. Proposed PCA+CE framework for unsupervised head–torso segmentation from a single 3D LiDAR frame.

A. Human 3D LiDAR Point Cloud Dataset

The study uses the KITTI Raw dataset [19], in which each frame contains a 3D LiDAR point cloud of a human subject walking toward or away from the sensor. Let the 3D LiDAR frame be the set of n spatial points P as in (1). The spatial coordinates (x, y, z) denote lateral, depth, and vertical direction relative to the sensor. The vertical extent of the body is divided into N_b horizontal slices with an interval defined in:

$$\Delta z = \frac{z_{min} - z_{max}}{N_s} \quad (2)$$

Each slice P_i contains all points within the height of the range $z_i - \Delta z < z_j \leq z_j$. Each frame is processed independently to ensure compatibility with a single scan system.

B. PCA Width Extraction

For each slice of P_i, the lateral coordinats (x, y) are used to measure cross-sectional spread. After centering by the centroid $\mu_i = [\overline{x}_i, \overline{y}_i]$, the covariance can be computed using:

$$C_1 = \frac{1}{m-1}\tilde{X}_i^T \tilde{X}_i \quad (3)$$

where $\tilde{X}_i = X_i - \mu_i$ and m is the number of points in the slice. The dominant eigenvalue λ_{max} of C_i represents the direction of the maximum variance, and the PCA width is defined in:

$$w(z_i) = 2\sqrt{\lambda_{max}} \quad (4)$$

This feature captures the macroscopic body shape, with a narrowing of the head and broader shape at the torso.

C. CE Estimation

To describe fine-grained 3D complexity, each point in the slice P_i is assigned a surface normal vector $n_j = [n_x, n_y, n_z]^T$. Local curvature is measured by the variation in normal directions between adjacent points. The CE $H(z_i)$ is defined as the mean squared deviation of these neighbouring normals, as shown in (5). Higher entropy values indicate disordered, rounded regions (such as the head), while lower values correspond to planar areas (chest or back). This means that spherical regions, such as the head, exhibit higher directional randomness among normals, whereas the torso remains largely planar with low entropy values:

$$H(z_i) = \frac{1}{m-1}\sum_{j=1}^{m-1} \| n_{j+1} - n_j \| \quad (5)$$

D. Feature Normalization and Fusion

The PCA width $w(z)$ and CE $H(z)$ are normalized to the range [0, 1] using the 5th and 95th percentiles to reduce outlier sensitivity, as defined in:

$$u_n = \frac{u - Pc_{5(u)}}{Pc_{95} - Pc_{5(u)} + \varepsilon}, u \in w, H, \varepsilon = 10^{-9} \quad (6)$$

Both descriptors are then fused into a single segmentation score, as shown in:

$$S(z) = \alpha w_n(z) + (1-\alpha) H_n(z) \quad (7)$$

where $\alpha = [0,1]$ balances the contribution of global (PCA) and local (curvature) features.

E. Adaptive Thresholding

The adaptive threshold S_{thr} is derived from the statistical distribution of $S(z)$, as given in:

$$S_{thr} = S_{top} + f(S_{torso} - S_{top}) \quad (8)$$

Where S_{top} and S_{torso} correspond to 30th and 70th percentiles, and f is the sensitivity factor. The boundary height z_{cut} is confirmed when $S(z)$ exceed S_{thr} for L consecutive slice, as described in:

$$S(z_i), S(z_{i+1}). \ldots, S(z_{i+L}) > S_{thr} \Rightarrow z_{cut} = z_i \quad (9)$$

Thus, the segmentation result is defined as:

$$Head\ if\ z \geq z_{cut}, Body\ if\ z \leq z_{cut} \quad (10)$$

F. Parameter Setting

Unless stated otherwise, the parameters used in this study are N_s = 28 vertical slices, α = 0.2, f = 0.4, and L = 3 in all experiments. Increasing N_s improves boundary resolution but may introduce instability when slices become sparse, and moderate values ≈ 24–32 provide a stable trade-off on KITTI frames. The fusion weight α controls the balance between global width and local curvature cues. A smaller α makes the score more curvature-driven, while a larger α approaches the PCA-only behavior. The factor f determines how conservative the threshold is, and L suppresses isolated spikes by requiring consistent evidence across slices. For CE computation, surface normals are estimated after voxel downsampling (0.02 m) using a hybrid neighborhood search (radius 0.05 m, max_{nn}= 30). These settings provide stable, normal estimates in sparse outdoor LiDAR while keeping computation lightweight.

IV. RESULTS AND DISCUSSION

To evaluate the effectiveness of the proposed PCA+CE segmentation method, a comparative analysis was conducted against a pure PCA-based baseline. The evaluation employed manually annotated ground truth labels using a binary classification criterion as defined in:

$$label_{p_i} = \begin{cases} 1, p_i \in Head \\ 0, p_i \in Body \end{cases} \quad (11)$$

The automatically segmented outputs were converted into the same binary format and compared with the ground truth using three standard metrics: precision, recall, and F1-score, as defined in:

$$\text{Precision} = \frac{TP}{TP+FP} \quad (12)$$

$$\text{Reacall} = \frac{TP}{TP+FN} \quad (13)$$

$$\text{F1} - \text{score} = \frac{2PR}{P+R} \quad (14)$$

where, *TP* denotes the number of correctly detected head points, *FP* represents body points misclassified as head, and *FN* corresponds to undetected head points.

The experimental evaluation utilized four raw 3D LiDAR sequences obtained from the KITTI Vision Benchmark Suite. Each sequence provides temporally ordered LiDAR scans captured using a Velodyne HDL-64E sensor at approximately 10 Hz, representing outdoor human walking scenarios. Among these, the datasets 2011_09_28_drive_0183 and 2011_09_28_drive_0174 were selected for detailed analysis due to their contrasting geometric perspectives. The 2011_09_28_drive_0183 depicts a pedestrian walking toward the LiDAR sensor, resulting in a gradual enlargement of the head–torso region in the 3D view, whereas 2011_09_28_drive_0174 captures the same subject walking away from the sensor, introducing gradual occlusion and decreasing point density at the upper body. This bidirectional configuration ensures a balanced evaluation under varying spatial occlusions and angular distortions caused by motion and scanning geometry. All frames were processed independently as static point clouds using the proposed segmentation pipeline. Each frame's head–body boundary was automatically computed, and its segmented results were compared with the manually annotated reference.

Quantitative comparison between the baseline PCA width method, CE method, and the proposed PCA+CE approach was carried out across all LiDAR frames in both motion scenarios,

which are toward the LiDAR sensor and away from the LiDAR sensor. The average performance metrics are summarized in Table I.

TABLE I. COMPARISON OF THE BASELINE AND PROPOSED METHODS

Methods	Precision	Recall	F1-score
PCA width (baseline)	0.845	0.886	0.841
CE (baseline)	0.802	0.854	0.763
PCA+CE (proposed)	0.847	0.914	0.844

Table I indicates that the proposed PCA+CE improves the overall trade-off between detection accuracy and completeness. Compared with the PCA-width baseline, PCA+CE slightly increases precision (0.845-0.847), indicating fewer false detections of non-head regions, while achieving a clearer gain in recall (0.886-0.914), suggesting that the head region is captured more completely without missing upper portions. In contrast, the CE-only baseline yields the lowest overall performance (F1-score = 0.763), confirming that local curvature cues alone are insufficient in sparse outdoor LiDAR and that a global geometric prior is still required to avoid shoulder/upper-torso confusion. Across frames, the mean ± std F1-score is 0.841 ± 0.306 for PCA and 0.844 ± 0.253 for PCA+CE. The reduced variability of PCA+CE is consistent with more stable boundary estimation under changing point density, occlusion, and viewing angle.

The proposed PCA+CE framework can be viewed as a targeted enhancement of conventional PCA slice width segmentation that addresses a known failure mode reported in prior geometric methods. Boundary drift occurs when the global width assumption is violated by rotation, shoulder overlap, or sparse sampling. By design, CE provides a complementary local cue that responds to surface orientation disorder, which tends to be higher in rounded head regions and lower in near-planar torso regions. The CE-only baseline results, outlined in Table I, further clarify this relationship. Local curvature cues alone are insufficient in sparse outdoor LiDAR with a lower F1-score, consistent with the sensitivity of curvature descriptors to sampling irregularities discussed in prior point cloud surface analysis. However, when fused with PCA width, CE acts as a lightweight stabilizer that improves recall while preserving precision, indicating that the global descriptor supplies a necessary shape prior while the local cue improves transition sensitivity. This behavior aligns with the broader trend in prior hybrid approaches, in which combining global structure and local surface cues improves robustness, while maintaining full interpretability and avoiding supervised learning or heavy optimization.

For qualitative illustration, Figure 2 presents only the PCA baseline and the proposed PCA+CE results, since the CE-only baseline exhibits inferior quantitative performance and would not add meaningful interpretive value to the visual comparison.

Although the numerical gains may appear modest, they are systematic and consistent across both approaching and receding motion scenarios, confirming that the introduction of CE provides a tangible geometric advantage. Such consistency across directional motion validates that the curvature component generalizes well to diverse point-of-view geometries. The curvature term effectively acts as a local stabilizer, mitigating fluctuations in PCA width that typically arise from body pose variation, angular misalignment, or LiDAR sampling noise. By capturing the micro-level irregularities in surface orientation, the method preserves the continuity of vertical segmentation even when the point density or incidence angle changes dynamically across frames.

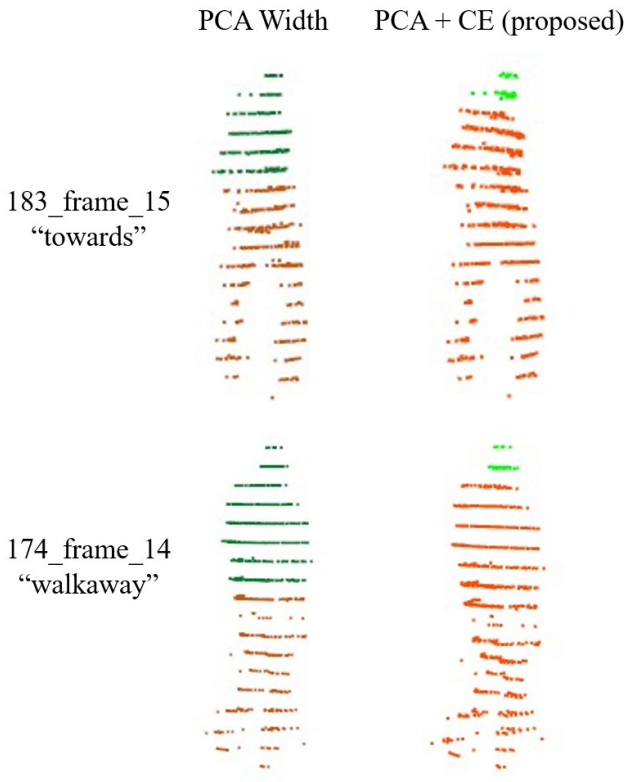

Fig. 2. Visual comparison between baseline PCA segmentation (left) and proposed PCA+CE segmentation (right) on KITTI 3D LiDAR frames.

This stabilizing effect enhances the vertical segmentation consistency without requiring any labeled data, statistical priors, or learning-based adaptation. CE serves as a structural regularizer that injects local shape awareness into the global PCA-based analysis. This allows the method to maintain robustness against common challenges in real-world 3D sensing, such as motion blur, point sparsity, and partial occlusion, while remaining fully unsupervised and computationally efficient.

Visual inspection corroborates these quantitative findings. As displayed in Figure 2, the proposed PCA+CE framework produces more anatomically coherent segmentation boundaries than the pure PCA baseline. The head region is more precisely isolated, with smoother boundary transitions and a noticeable reduction in misclassified shoulder or neck points. Across multiple temporal frames, the PCA+CE method maintains the segmentation boundary even in oblique and walking poses where the PCA-only approach tends to drift or over-segment the torso.

Overall, the incorporation of CE not only refines local decision stability but also introduces a meaningful improvement in global interpretability. The resulting segmentation is both geometrically faithful and statistically consistent, providing a reliable foundation for downstream tasks such as pose estimation, human tracking, and 3D behavior analysis.

V. CONCLUSION

The proposed Curvature Entropy-Enhanced Principal Component Analysis (PCA+CE) framework demonstrates measurable and interpretable improvements in Three-Dimensional (3D) LiDAR-based human head–body segmentation. By integrating local CE with global PCA geometry, the method achieves enhanced vertical segmentation stability and inter-frame consistency. The CE term introduces a localized sensitivity absent in standard PCA, enabling the system to detect the head–torso transition without relying solely on macroscopic geometric width.

Compared with the pure PCA baseline, PCA+CE increases the overall F1-score from 84.1% to 84.4% (+0.36%), while preserving computational efficiency and full interpretability and requiring no labeled data, additional annotations, or learning-based training. These findings are consistent with prior insights in geometric segmentation that the combination of global shape cues and local surface descriptors improves robustness, while the proposed approach remains fully unsupervised and lightweight for sparse LiDAR frames. The improvement is consistent across both evaluated motion scenarios ("toward" and "away"), and the estimated head–torso boundary Z_{cut} is qualitatively more stable under mild rotations and posture changes.

However, the study has two key limitations. First, the accuracy of the proposed framework depends on the number of vertical slices; substantial variation in subject height may cause minor segmentation shifts. Second, the adaptive thresholding process currently operates on a per-frame basis, without incorporating temporal continuity between consecutive scans. Future work will extend this approach by integrating temporal smoothing and dynamic entropy modeling to enhance robustness in continuous LiDAR sequences.

ACKNOWLEDGMENT

The authors would like to thank the Institut Teknologi Sepuluh Nopember, Surabaya, Indonesia, for supporting this work.

REFERENCES

[1] S. Ibrayev and B. Omarov, "Designing an Autonomous Mobile Robot Featuring Self-Localization through 3D LiDAR Technology," *Engineering, Technology & Applied Science Research*, vol. 15, no. 5, pp. 28224–28231, Oct. 2025, https://doi.org/10.48084/etasr.13014.

[2] J. Gómez, O. Aycard, and J. Baber, "Efficient Detection and Tracking of Human Using 3D LiDAR Sensor," *Sensors*, vol. 23, no. 10, May 2023, Art. no. 4720, https://doi.org/10.3390/s23104720.

[3] S. Y. Alaba and J. E. Ball, "A Survey on Deep-Learning-Based LiDAR 3D Object Detection for Autonomous Driving," *Sensors*, vol. 22, no. 24, Dec. 2022, Art. no. 9577, https://doi.org/10.3390/s22249577.

[4] C. R. Qi, L. Yi, H. Su, and L. H. Guibas, "PointNet++: Deep Hierarchical Feature Learning on Point Sets in a Metric Space," in *31st Conference on Neural Information Processing Systems*, Long Beach, CA, USA, 2017.

[5] J. Yang, L. El Mendili, Y. Khayer, S. McArdle, and L. Hashemi Beni, "Instance Segmentation of LiDAR Data with Vision Transformer Model in Support Inundation Mapping Under Forest Canopy Environment," *The International Archives of the Photogrammetry, Remote Sensing and Spatial Information Sciences*, vol. XLVIII-1/W2-2023, pp. 203–208, Dec. 2023, https://doi.org/10.5194/isprs-archives-XLVIII-1-W2-2023-203-2023.

[6] N. E. Budiyanta, E. M. Yuniarno, and M. H. Purnomo, "Human Sliced Feature-Based Head Segmentation on 3D LiDAR Point Cloud Data," in *28th International Computer Science and Engineering Conference*, Nov. 2024, pp. 1–5, https://doi.org/10.1109/ICSEC62781.2024.10770637.

[7] C.-H. Lin, J.-Y. Chen, P.-L. Su, and C.-H. Chen, "Eigen-Feature Analysis of Weighted Covariance Matrices for LiDAR Point Cloud Classification," *ISPRS Journal of Photogrammetry and Remote Sensing*, vol. 94, pp. 70–79, Aug. 2014, https://doi.org/10.1016/j.isprsjprs.2014.04.016.

[8] N. E. Budiyanta, E. M. Yuniarno, and M. H. Purnomo, "Human Point Cloud Data Segmentation based on Normal Vector Estimation using PCA-SVD Approaches for Elderly Activity Daily Living Detection," in *TENCON 2021-IEEE Region 10 Conference*, Auckland, New Zealand, Dec. 2021, pp. 632–636, https://doi.org/10.1109/TENCON54134.2021.9707317.

[9] X. Zhan, Y. Cai, and P. He, "A Three-Dimensional Point Cloud Registration Based on Entropy and Particle Swarm Optimization," *Advances in Mechanical Engineering*, vol. 10, no. 12, Dec. 2018, Art. no. 1687814018814330, https://doi.org/10.1177/1687814018814330.

[10] Z. Yu, T. Wang, T. Guo, H. Li, and J. Dong, "Robust Point Cloud Normal Estimation via Neighborhood Reconstruction," *Advances in Mechanical Engineering*, vol. 11, no. 4, Apr. 2019, Art. no. 1687814019836043, https://doi.org/10.1177/1687814019836043.

[11] H. Hoppe, T. DeRose, T. Duchamp, J. McDonald, and W. Stuetzle, "Surface Reconstruction from Unorganized Points," *ACM SIGGRAPH Computer Graphics*, vol. 26, no. 2, pp. 71–78, Jul. 1992, https://doi.org/10.1145/142920.134011.

[12] N. J. Mitra and A. Nguyen, "Estimating Surface Normals in Noisy Point Cloud Data," in *Proceedings of the nineteenth annual symposium on Computational geometry*, San Diego, CA, USA, Jun. 2003, pp. 322–328, https://doi.org/10.1145/777792.777840.

[13] Q. Mérigot, M. Ovsjanikov, and L. J. Guibas, "Voronoi-Based Curvature and Feature Estimation from Point Clouds," *IEEE Transactions on Visualization and Computer Graphics*, vol. 17, no. 6, pp. 743–756, Jun. 2011, https://doi.org/10.1109/TVCG.2010.261.

[14] T. Fiolka, J. Stückler, D. A. Klein, D. Schulz, and S. Behnke, "SURE: Surface Entropy for Distinctive 3D Features," in *Spatial Cognition VIII*, vol. 7463, C. Stachniss, K. Schill, and D. Uttal, Eds. Berlin, Germany: Springer Berlin Heidelberg, 2012, pp. 74–93.

[15] G. Wang, L. Wu, Y. Hu, and M. Song, "Point Cloud Simplification Algorithm Based on the Feature of Adaptive Curvature Entropy," *Measurement Science and Technology*, vol. 32, no. 6, Jun. 2021, Art. no. 065004, https://doi.org/10.1088/1361-6501/abd497.

[16] D. Wu, Z. Liang, and G. Chen, "Deep Learning for LiDAR-Only and LiDAR-Fusion 3D Perception: A Survey," *Intelligence & Robotics*, vol. 2, no. 2, pp. 105–129, 2022, https://doi.org/10.20517/ir.2021.20.

[17] L. Xiao, R. Wang, B. Dai, Y. Fang, D. Liu, and T. Wu, "Hybrid Conditional Random Field Based Camera-LiDAR Fusion for Road Detection," *Information Sciences*, vol. 432, pp. 543–558, Mar. 2018, https://doi.org/10.1016/j.ins.2017.04.048.

[18] S. Ural and J. Shan, "Min-Cut Based Semantic Building Labeling for Airborne LiDAR Data," *ISPRS Annals of the Photogrammetry, Remote Sensing and Spatial Information Sciences*, vol. V-2–2020, pp. 305–312, Aug. 2020, https://doi.org/10.5194/isprs-annals-V-2-2020-305-2020.

[19] A. Geiger, P. Lenz, C. Stiller, and R. Urtasun, "Vision Meets Robotics: The KITTI Dataset," *The International Journal of Robotics Research*, vol. 32, no. 11, pp. 1231–1237, Sep. 2013, https://doi.org/10.1177/0278364913491297.